

Effect of laser pulse shaping parameters on the fidelity of quantum logic gates

Ryan R. Zaari and Alex Brown

Citation: *J. Chem. Phys.* **137**, 104306 (2012); doi: 10.1063/1.4747703

View online: <http://dx.doi.org/10.1063/1.4747703>

View Table of Contents: <http://jcp.aip.org/resource/1/JCPSA6/v137/i10>

Published by the [American Institute of Physics](#).

Additional information on *J. Chem. Phys.*

Journal Homepage: <http://jcp.aip.org/>

Journal Information: http://jcp.aip.org/about/about_the_journal

Top downloads: http://jcp.aip.org/features/most_downloaded

Information for Authors: <http://jcp.aip.org/authors>

ADVERTISEMENT



AIP Advances

Special Topic Section:
PHYSICS OF CANCER

Why cancer? Why physics? [View Articles Now](#)

Effect of laser pulse shaping parameters on the fidelity of quantum logic gates

Ryan R. Zaari and Alex Brown^{a)}

Department of Chemistry, University of Alberta, Edmonton, Alberta T6G 2G2, Canada

(Received 25 June 2012; accepted 9 August 2012; published online 11 September 2012)

The effect of varying parameters specific to laser pulse shaping instruments on resulting fidelities for the ACNOT₁, NOT₂, and Hadamard₂ quantum logic gates are studied for the diatomic molecule ¹²C¹⁶O. These parameters include varying the frequency resolution, adjusting the number of frequency components and also varying the amplitude and phase at each frequency component. A time domain analytic form of the original discretized frequency domain laser pulse function is derived, providing a useful means to infer the resulting pulse shape through variations to the aforementioned parameters. We show that amplitude variation at each frequency component is a crucial requirement for optimal laser pulse shaping, whereas phase variation provides minimal contribution. We also show that high fidelity laser pulses are dependent upon the frequency resolution and increasing the number of frequency components provides only a small incremental improvement to quantum gate fidelity. Analysis through use of the pulse area theorem confirms the resulting population dynamics for one or two frequency high fidelity laser pulses and implies similar dynamics for more complex laser pulse shapes. The ability to produce high fidelity laser pulses that provide both population control and global phase alignment is attributed greatly to the natural evolution phase alignment of the qubits involved within the quantum logic gate operation. © 2012 American Institute of Physics. [<http://dx.doi.org/10.1063/1.4747703>]

I. INTRODUCTION

Promising experimental implementations of quantum computing platforms, within the facet of chemistry, come in the form of nuclear magnetic resonance (NMR)¹⁻³ and ion traps.^{4,5} Within NMR an ensemble of molecules is excited via tuned electromagnetic pulses. Current linear ion trap quantum computer implementations use the shaped laser pulses to control individual atoms,⁶ although trapping approaches have been proposed and are currently being extended to molecules.^{7,8} Instead of exciting hyperfine states or atomic transitions, a complementary approach involves the control of the rovibrational states of a diatomic molecule (*diatomic quantum computing*).⁹ In this method, a mid-infrared laser pulse is shaped through a closed-loop feedback¹⁰⁻¹² mechanism to represent each specific quantum gate operation, through diatomic rovibrational state qubit excitations. Experimentally, the use of internal degrees of freedom of diatomic molecules for quantum computing has not received much attention. Two possible implementations using Li₂ (Ref. 13) and I₂ (Ref. 14) have been presented and neither utilized a closed-loop feedback loop for optimization. The two experiments implemented the quantum algorithms directly, termed *problem-specific* quantum computing, whereas the approach of interest in our studies is *universal* quantum computing, where in principle any quantum algorithm can be implemented.¹³ In order for future closed-loop feedback experiments to be realized, further theoretical investigations on the requirements for experimental implementations will be useful.

The majority of theoretical studies within diatomic quantum computing, using shaped laser pulses, produce excellent qubit control but with laser pulses that are difficult, or perhaps impossible, to realize experimentally and/or only show proof of principle applications on a particular choice of diatomic molecule.¹⁵⁻³⁰ In contrast, we previously studied the performance of shaped laser pulses on a general model diatomic³¹ and the ability to achieve high control with laser pulses having very few parameters (binary pulse shaping).³² The theoretical optimizing or shaping of laser pulses generally comes in two forms: optimal control theory (OCT)^{33,34} and genetic algorithm (GA)¹¹ optimization. Unless specific constraints are applied, OCT optimization can produce large intensities, a large range of frequency components (depending on the rotational, vibrational and/or electronic transitions available) and experimentally inaccessible pulse shapes.³⁵⁻³⁷ On the other hand, the GA can be incorporated into an experimental closed-loop feedback setup and thus theoretical implementation allows for an appropriate description of the possible laser pulses shapes. While the molecular structure is clearly important,³¹ it is also necessary to explore the limitations of the laser pulse shaping apparatus within the context of this specific application.

The aforementioned experimental implementations using Li₂ and I₂ had a laser pulse shaping setup that utilized a liquid crystal spatial light modulator (LC-SLM). A transform-limited (TL) pulse is incident upon a diffraction grating and the LC-SLM is illuminated by the resulting frequency spectrum. The output laser frequencies from the LC-SLM are recombined to form the shaped laser pulse. The LC-SLM contains a series of pixels that can independently control the amplitude and phase at each specific frequency resolution,

^{a)}E-mail: alex.brown@ualberta.ca.

and thus provides a multitude of various laser pulse shapes. The GA is used to determine the optimal combination of amplitude and phase at each frequency component in order to implement the desired quantum gate operation. We have implemented an analogous theoretical framework, which was also used in our previous works.^{31,32}

The object of the study detailed herein is to elucidate the importance of some adjustable parameters within a typical LC-SLM, namely (i) the effect of varying the LC-SLM pixel frequency resolution ($d\nu$), (ii) effective variance of the amplitude (A_j), (iii) phase (ϕ_j) at each pixel, and (iv) the effect of changing the number of pixels (n) included within the laser pulse shaping. Each of these four important parameters affects the total number of laser pulse combinations and thus the total size of the parameter space that needs to be explored to find the optimal laser pulse. It is important to have a parameter space of minimal size such that the GA can locate the optimal laser pulse with confidence and within an appropriate amount of computational time. A minimum parameter space requires a balance between the number of pulse shaping parameters and a maximum laser pulse fidelity, and hence the current study. In the present work, laser pulses are optimized to represent three common quantum gates (ACNOT₁, NOT₂, Had₂) on the rovibrational state qubits of carbon monoxide (¹²C¹⁶O). Building from our³¹ and others¹⁸ previous work using GA laser pulse optimization on CO, we demonstrate the effect of laser pulse shaping parameters on the ability to produce optimal laser pulses.

II. THEORY

The time-dependent Schrödinger equation (TDSE) can be written in matrix notation with time-dependent coefficients $c_{\nu J}(t)$:

$$\dot{\underline{c}}(t) = -\frac{i}{\hbar} [\underline{E} - \epsilon(t)\underline{\mu}] \underline{c}(t). \quad (1)$$

In Eq. (1), $\underline{c}(t)$ is the column vector of time-dependent rovibrational state coefficients, \underline{E} is the rovibrational state energy matrix, $\epsilon(t)$ is the linearly polarized electric field of the laser pulse and $\underline{\mu}$ is the rovibrational transition dipole matrix. The TDSE is solved using the Runge-Kutta fourth order method with 2²⁰-2²² time points depending on the pulse duration. The number of time points chosen is determined by an incremental change until a convergence threshold is met, based upon the total population after pulse interaction. There is a tradeoff between the selected convergence threshold and the computational time required for each calculation.

A. Model system

We restrict our study to the diatomic carbon monoxide (¹²C¹⁶O) with excitations occurring between rovibrational states according to vibrational excitation $\Delta\nu = \pm 1$ and rotational excitation $\Delta J = \pm 1$. The CO model consists of 7 vibrational states ($0 \leq \nu \leq 6$) each with 9 rotational states ($0 \leq J \leq 8$) for a total of 63 rovibrational states. With the energy contained in the laser pulses being optimized, rovibrational states higher than those used in the study were insignificantly pop-

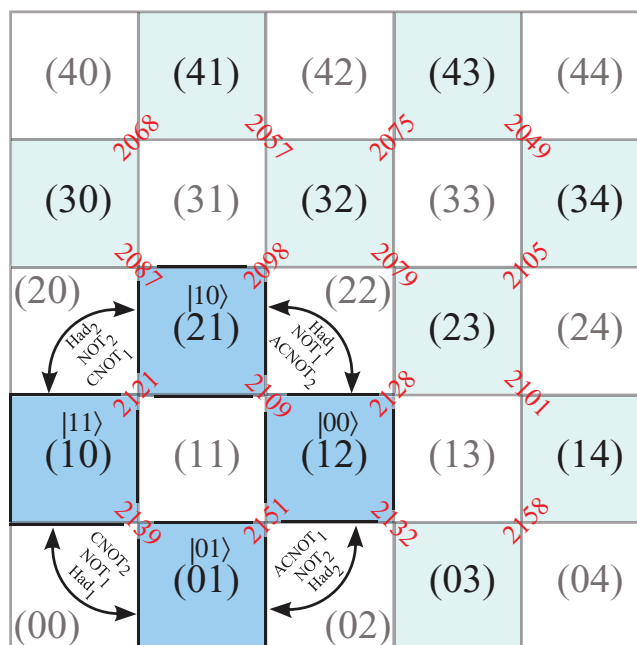


FIG. 1. Illustration of the first 12 accessible rovibrational states (shaded light blue boxes) of ¹²C¹⁶O labeled as (ν, J). The chosen qubit representations (shaded dark blue boxes) are labeled as $|q_1 q_2\rangle$. Available transitions are governed by the following simultaneous vibrational and rotational transitions: $\Delta\nu = \pm 1$ and $\Delta J = \pm 1$ which are illustrated by states connected along a diagonal. Some rovibrational states are inaccessible (white boxes). Excitation frequencies (red text) are in cm^{-1} and lie between the accessible rovibrational states. The qubits ($|00\rangle, |01\rangle, |10\rangle, |11\rangle$) that undergo a state change (black arrows) during an applied quantum gate operation, according to Table I, are labeled by the corresponding gate. Notice that the NOT and Hadamard gates require simultaneous control of 2 transitions. Reprinted with permission from R. R. Zaari and A. Brown, J. Chem. Phys. **132**, 014307 (2010). Copyright 2010, American Institute of Physics.

ulated and thus the reduced set used in this study is adequate. The four rovibrational states (ν, J) used to represent the qubits $|q_1 q_2\rangle$ are $|00\rangle \equiv (1, 2)$, $|01\rangle \equiv (0, 1)$, $|10\rangle \equiv (2, 1)$, and $|11\rangle \equiv (1, 0)$. Refer to Figure 1 for a detailed illustration containing the qubits, rovibrational states, and transition frequencies involved. The rovibrational state energies were determined by Mantz *et al.*³⁸ by fitting of experimental measurements of 1514 vibration-rotation and pure rotation transitions to a power series of vibrational and rotational quantum numbers - the energies fit both high ν ($\nu \leq 37$) and high J ($J \leq 100$) data within experimental uncertainty. The transition dipole moments were taken from the work of Goorvitch and Chackerian³⁹ in which experimental data was fit to a polynomial in terms of the angular quantum number.

B. Quantum logic gates

In the present study three quantum logic gates were studied: the alternative controlled-NOT (ACNOT₁) gate, NOT₂ gate, and Hadamard 2 (Had₂) gate. The qubit operations for each gate are depicted in Table I. The subscript “1” of the ACNOT₁ gate is used to denote the control qubit, here q_1 , and subsequent flip of the target qubit q_2 when $q_1 = 0$. In the case of the NOT₂ and Had₂ gates, the subscript “2” simply denotes a flip of qubit 2 (q_2). Laser pulses are to be shaped in order to implement the state transformations required for each

TABLE I. Quantum gate operations which are implemented by an optimized laser pulse in this study with qubit representation $|q_1 q_2\rangle$. NOT₂/ Had₂: The qubit flip occurs on qubit 2 (q_2). ACNOT₁: The control qubit is q_1 and the qubit flip occurs on the target qubit q_2 when $q_1 = 0$.

ACNOT ₁ :	$ 10\rangle \rightarrow 10\rangle$	NOT ₂ :	$ 00\rangle \leftrightarrow 01\rangle$
	$ 11\rangle \rightarrow 11\rangle$		$ 10\rangle \leftrightarrow 11\rangle$
	$ 00\rangle \leftrightarrow 01\rangle$		
Had ₂ :	$ 00\rangle \leftrightarrow \frac{1}{\sqrt{2}}(00\rangle + 01\rangle)$		
	$ 01\rangle \leftrightarrow \frac{1}{\sqrt{2}}(00\rangle - 01\rangle)$		
	$ 10\rangle \leftrightarrow \frac{1}{\sqrt{2}}(10\rangle + 11\rangle)$		
	$ 11\rangle \leftrightarrow \frac{1}{\sqrt{2}}(10\rangle - 11\rangle)$		

quantum gate operation. Thus each quantum gate operation will have a unique laser pulse and each laser pulse will have an associated value describing its ability to perform the quantum gate operation, termed the *fidelity* (see Sec. II C).

C. Laser pulse optimization

The present study investigates features of experimental pulse shaping using a LC-SLM where shaping occurs in the frequency domain. The LC-SLM produces a discretized frequency spectrum, $\epsilon(v_j)$, given by

$$\epsilon(v_j) = \epsilon_0 \sqrt{A(v_j)} \exp \left[-2 \ln 2 \left(\frac{v_j - v_0}{\Delta v} \right)^2 \right] \exp[i\phi(v_j)], \quad (2)$$

where ϵ_0 is the peak field strength, v_0 is the central frequency, $\Delta v = 100 \text{ cm}^{-1}$ is the full width at half-maximum pulse width and v_j represents the discrete frequencies at which the field is shaped. The amplitude and phase range from $0 \leq A(v_j) \leq 1$ and $0 \leq \phi(v_j) \leq 2\pi$, respectively. Variation in amplitude or phase is accomplished by dividing up the respective ranges of each parameter by a select n number of segments. The notation used to describe the number of segment divisions is for amplitude nA variations and for phase $n\phi$ variations. In the case of binary pulse shaping (a choice of $2A$ and 2ϕ), $A = 0$ or 1 and $\phi = 0$ or π . A transform limited (TL) pulse results when $A = 1$ and $\phi = 0$ for all frequency components, v_j , of Eq. (2). Typically, in order to obtain the time-domain laser pulse from this frequency domain spectrum, a Fourier transform is used. An analytic form for the time-domain laser pulse, $\epsilon(t)$, has been derived from the discretized frequency spectrum, $\epsilon(v_j)$ (see the Appendix),

$$\epsilon(t) = \text{sinc}(\pi t d\nu) \sum_{j=0}^n A'_j \cos(2\pi v_j t + \phi_j), \quad (3)$$

where $A'_j = d\nu \epsilon_0 \sqrt{A_j} e^{-2 \ln 2 \left(\frac{v_j - v_0}{\Delta v} \right)^2}$ and contains variables as described in Eq. (2). The frequency resolution is labeled by $d\nu$ and the summation occurs over n discretized frequency components. The symmetry of resulting laser pulses can be deduced using Eq. (3). The *sinc* function is symmetric along the pulse duration from $-\frac{T}{2} \leq t \leq \frac{T}{2}$. As long as the phase at each frequency component (ϕ_j) of the cosine function varies only by $\phi = 0$ or $\phi = \pi$, where $\cos(2\pi v_j t + \pi) = -\cos(2\pi v_j t)$, then overall the resulting laser pulse shapes

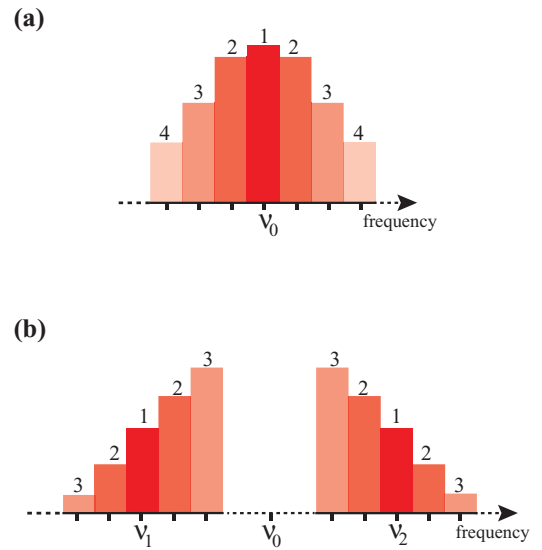


FIG. 2. Illustration of the incremental addition of frequency components for the ACNOT₁, NOT₂, and Had₂ gates. (a) ACNOT₁ gate. One frequency component at “1,” the central frequency v_0 . Three frequency components at “1” and “2.” Five frequency components at “1,” “2,” and “3.” Seven frequency components at “1,” “2,” “3,” and “4.” The addition of more frequency components continues in this manner. (b) NOT₂ and Had₂ gates. Two frequency components at “1,” with the transition frequencies v_1, v_2 . Six frequency components at “1” and “2.” Ten frequency components at “1,” “2,” and “3.” The addition of more frequency components continues in this manner.

will be symmetric in time. Moreover, a symmetric pulse shape guarantees that the resulting phases of the set of two qubit transitions of the quantum gate operation will be the same. For example, a symmetric laser pulse being shaped to represent the ACNOT₁ gate will result in the qubits $|00\rangle$ and $|01\rangle$ being in phase. This effect of temporally symmetric laser pulses was originally documented by Schröder and Brown.³⁶

The ACNOT₁ gate requires only one frequency for the state-to-state transition between $|00\rangle$ and $|01\rangle$, as shown in Table I. This frequency for ¹²C¹⁶O is $v_0 = 2151 \text{ cm}^{-1}$ and also corresponds to the central frequency of the Gaussian envelope used for laser pulse shaping of the ACNOT₁ gate. The NOT₂ and Had₂ gates require two frequencies for each of the state-to-state transitions between $|00\rangle$ and $|01\rangle$, and $|10\rangle$ and $|11\rangle$. These frequencies are at $v_2 = 2151 \text{ cm}^{-1}$ and $v_1 = 2121 \text{ cm}^{-1}$, respectively. The central frequency of the Gaussian envelope spanning these two frequencies is $v_0 = 2136 \text{ cm}^{-1}$ and corresponds to the average between the two transitions involved in the NOT₂ or Had₂ gate operations. The relative positioning of these frequencies is illustrated in Figure 2. Note that the central frequency used for the ACNOT₁ gate is different than that used for the NOT₂ and Had₂ gates. Also shown in the figure is the method by which additional frequencies are added to the laser pulse shaper for the ACNOT₁ gate (Figure 2(a)) and for the NOT₂ and Had₂ gates (Figure 2(b)). Additional frequency components are added on either side of the transition frequencies involved in the qubit excitations.

With reference to Eq. (3) the variables we are manipulating within this study are A_j (amplitude), ϕ_j (phase), n (number of frequency components), and $d\nu$ (frequency resolution). These four parameters will produce different laser

pulse shapes and thus different rovibrational state qubit dynamics. In order to optimize a pulse shape for performing a particular quantum gate operation, a GA is utilized.⁴⁰ The GA uses evolutionary strategies from biology such as natural selection and survival of the fittest to search the parameter space of possible laser pulse shapes and find the appropriate one, without having to sample all combinations. In the results reported here, we use between 25 and 1000 generations each consisting of 16 individuals and a micro-GA subroutine. The micro-GA eliminates *inbreeding*, which is the case when individual laser pulses become too similar, by keeping the best individual and randomly selecting 15 new individuals to create a new generation. The chosen number of generations was determined based upon the relative size of the parameter space. For example, the ACNOT₁ gate with a parameter space consisting of a single frequency component ($n = 1$) with 16 amplitude (16A) and 2 phase (2ϕ) choices would consist of $(16 \times 2)^1 = 32$ possible laser pulse combinations. If the same quantum gate had a parameter space consisting of 13 frequency components ($n = 13$), 32A, and 2ϕ , then it would produce $(32 \times 2)^{13} = 3.02 \times 10^{23}$ laser pulse combinations! A large number of generations would be required for the latter case to ensure appropriate sampling of the parameter space and to ensure confidence of the optimal solution being found.

In order for the GA to know how well an individual (laser pulse) performs the desired quantum gate operation, a fitness function is needed. The form of the fitness function, in this case termed the *fidelity* (F), used in the present work is

$$F = \frac{1}{N^2} \left| \sum_{k=1}^N \langle \Psi_k(T) | \Phi_k \rangle \right|^2, \quad (4)$$

where $\Psi_k(T)$ is the resulting wavefunction after the laser pulse has been applied, T is the total laser pulse duration, and Φ_k is the target wavefunction. The wavefunctions are summed over the number of transitions required by the quantum gate, $N = 4$ here, and then divided by a normalization factor, N^2 , to ensure the fidelity ranges between 0 and 1. The fidelity is dependent upon the phase alignment of all the qubits, which can be explicitly viewed in an alternative representation of the fidelity,

$$F = \frac{1}{N^2} \left[\sum_k |r_k|^2 + 2 \sum_{k \neq k'} r_k r_{k'} \cos(\Delta\phi_{kk'}) \right]. \quad (5)$$

For simplicity, the time-dependent wavefunctions (Eq. (4); $\Psi_k(T)$, Φ_k) are written in complex Euler notation, i.e., $\Psi_k = r_k e^{i\phi_k}$ and Φ_k are assumed to be real. The term r_k describes the magnitude of the time-dependent coefficients corresponding to wavefunctions Ψ_k at the end of the laser pulse interaction. $\Delta\phi_{kk'}$ is the difference between qubit phases, ϕ_k and $\phi_{k'}$, at the end of the laser pulse duration.

Another description of the dynamics occurring during the laser pulse/molecule interaction, but not used as a means for optimization, is the average population, \bar{P} ,

$$\bar{P} = \frac{1}{N} \sum_{k=1}^N |\langle \Psi_k(T) | \Phi_k \rangle|^2. \quad (6)$$

The average population (\bar{P}) describes the ability of the laser pulse to excite from an initial state to a final state as deemed by the quantum gate operation. The average population is not dependent upon the final phase of the qubits. A requirement of molecular quantum computing is *global phase alignment*.^{27,41} The final phases of each qubit after the total pulse interaction time must be the same. This ensures that the application of subsequent quantum gate operations (laser pulses) occurs without inducing a phase discrepancy and thus decreasing the effectiveness of the quantum gate. Hence, the fidelity is used as the fitness function for GA optimizations rather than the average population (\bar{P}). Global phase alignment is related to the second term of Eq. (5).

III. RESULTS AND DISCUSSION

This investigation was carried out in three parts in order to examine the effects on fidelity of variations to amplitude (A_j), phase (ϕ_j), number of frequency components (n), and frequency resolution ($d\nu$) or synonymously total pulse duration (T). Each has a particular role in producing an optimal pulse shape based upon the experimental discretized pulse shaping LC-SLM. The variations to the laser pulse shaping parameters were carried out on the ACNOT₁, NOT₂, and Had₂ quantum logic gates and their effects on the resulting quantum logic gate Fidelity (F) were evaluated. The three sections are as follows:

A. Effect of total pulse duration (F vs. T)

At a constant total pulse energy, the total pulse duration, T , was varied. The total pulse energy for each quantum gate was taken from our previous work.³² The frequency resolution ($d\nu$) and total pulse duration (T) are related by $d\nu = \frac{2}{T}$. As a result, a qualitative relationship between the total pulse duration, T and areas of high and low fidelity can be deduced. The laser pulse included only the single transition frequency (ACNOT₁) or only two frequencies (NOT₂ and Had₂), depending upon the quantum gate. Binary pulse shaping ($A = 0$ or 1 , $\phi = 0$ or π) was utilized.

B. Effect of laser pulse energy (F vs. A)

The low fidelities obtained in Sec. III A, as detailed in the paragraph above, may be associated with pulse shapes of non-optimal total pulse energy. By determining optimal amplitudes at the excitation frequency (see Figure 2(a); ν_0) or frequencies (see Figure 2(b); ν_1, ν_2), the appropriate pulse shape of optimal energy can be generated. At specifically chosen values of total pulse duration, T , the number of amplitude components was varied beyond two choices (the phase variation remained at 2ϕ), from $2A$ until appropriate convergence was reached at $512A$. Thus, the total pulse energy available to all frequency components can be controlled at each frequency component by amplitude variation.

C. Effect of frequency resolution, amplitude, and phase (F vs. n, A, ϕ)

Finally, in order to further investigate the effect of laser pulse parameters on increasing the resulting fidelity, the number of frequency components (n) was increased

beyond the excitation frequency, ν_0 (see Figure 2(a)) or frequencies, ν_1 and ν_2 (see Figure 2(b)). Concurrently, the number of amplitude (A) or phase (ϕ) values was increased from only two choices to having 32 choices each (i.e., $32A$ or 32ϕ). This investigation was carried out on the pulses of optimal energy, as determined in Sec. III B and detailed in the previous paragraph, of a single chosen total pulse duration for each quantum gate operation.

A. Effect of total pulse duration (F vs. T)

In order to examine the effect of the total pulse duration on the fidelity, a scan of the frequency resolution ($d\nu$) was carried out by setting the total frequency window to 500 cm^{-1} and discretizing the window into odd integer values (x) for $d\nu = \frac{500}{x-1}$ but there was no direct optimization. Thus, the total pulse duration (T) at intervals of $\Delta T = 0.27 \text{ ps}$ for $5.34 \text{ ps} \leq T \leq 66.71 \text{ ps}$ was sampled. The laser pulse energies for each quantum gate were constant and chosen based upon the TL-pulse energies from our previous work.³² For these simulations, laser pulses were constructed from all combinations of amplitude and phase from $A = 0$ or 1 and $\phi = 0$ or π for each quantum gate. The fidelity for each laser pulse at each value of $d\nu$ was calculated and then $d\nu$ was converted to the corresponding value for the total pulse duration. From this point on, references to the total pulse duration T should be considered synonymous to the frequency resolution $d\nu$. The field free case, for the NOT₂ and Had₂ gates when $\epsilon(t) = 0$, is omitted since it produces a fidelity of zero due to the nature of the excitations involved (see Table I). In comparison, the ACNOT₁ gate when $\epsilon(t) = 0$ produces a maximum fidelity of $F = 0.25$. Similar information about the relationship between the fidelity and total pulse duration could be determined experimentally by scanning through values of $d\nu$ and optimizing a laser pulse for each value when $A = 0$ or 1 and $\phi = 0$ or π .

1. ACNOT₁ quantum gate

The total pulse energy was kept constant at $E = 10 \mu\text{J}$ and the central frequency is $\nu_0 = 2151 \text{ cm}^{-1}$. Three unique laser pulses at each pulse duration T can be produced. Using the notation $[A, \phi]$, they are $[1, \pi]$, $[1, 0]$, and the field free case $[0, \phi]$. The fidelities for these three pulses as a function of pulse duration are shown in Figure 3. As seen in Figure 3, there are six locations where the fidelity is highest, though the pattern may repeat itself in time. The two laser pulses, $[1, \pi]$ and $[1, 0]$, share a relationship such that the maximum fidelity alternates between each other as T is increased (see the inset of Figure 3), where the fidelities from $6.5 \text{ ps} \leq T \leq 8.8 \text{ ps}$ are plotted. The overall pattern of maximum fidelities produced by $[1, \pi]$ and $[1, 0]$ follows the trend of fidelity for the field free scenario (solid blue line), though not all cases result in a global maximum fidelity (e.g., $T = 22.7 \text{ ps}$ and 45.1 ps). When $\epsilon(t) = 0$ in the field free case (Figure 3; solid blue line) the excitation $|00\rangle \leftrightarrow |01\rangle$ cannot occur and thus the fidelity represents the phase alignment of qubits $|11\rangle$ and $|10\rangle$. It seems that the free evolution phase alignment of qubits $|11\rangle$ and $|10\rangle$ determines whether a high fidelity can be obtained for a specific value of $d\nu$. The exception being the unexpectedly low fidelities at $T = 22.7 \text{ ps}$ and

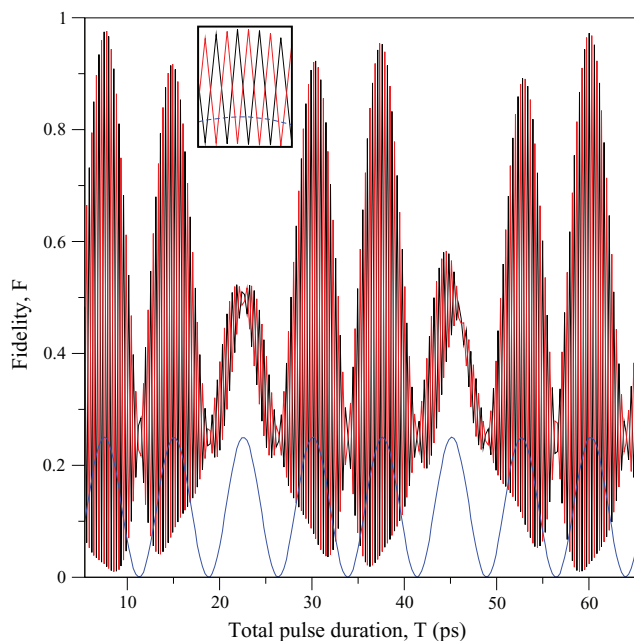


FIG. 3. Plot of the resulting fidelities for three pulse shapes as a function of the total pulse duration T for the ACNOT₁ quantum gate having a total pulse energy of $10 \mu\text{J}$. The laser pulses, consist of 1 frequency component ($n = 1$) at the transition frequency (2151 cm^{-1}) with a choice of amplitude $2A$ and phase 2ϕ using the notation $[A\phi]$, are $[1, \pi]$ black line, $[1, 0]$ red line, and $[0, 0]$ blue line. The inset shows the alternating fidelity between $[1, \pi]$ and $[1, 0]$ for $6.5 \text{ ps} \leq T \leq 8.8 \text{ ps}$.

45.1 ps . Analysis of the results for these two low fidelity local maxima is detailed in Sec. III B.

The fidelity of the free evolution of qubits $|10\rangle$, and $|11\rangle$ is described by, $F = \frac{1}{16}[2 + 2 \cos(\Phi_{|11\rangle} - \Phi_{|10\rangle})]$, where $\Phi_{|q_1q_2\rangle}$ is the final phase for qubit $|q_1q_2\rangle$ after the pulse interaction. As seen in Figure 3, the maximum fidelity (peaks) occur at intervals every $T = 7.526 \text{ ps}$. The free evolution alignment between qubits $|10\rangle$ and $|11\rangle$ is related to the energy difference between these states and occurs at a frequency of 2121 cm^{-1} (63.57 ps^{-1}). This is much larger than the peak oscillation period of $\frac{1}{7.526} = 0.1329 \text{ ps}^{-1}$ just stated. However, the period observed in Figure 3 is simply a result of the pulse duration (frequency resolution) sampling used in the present work. When the free evolution frequency of these qubits is sampled at the pulse duration interval used in these calculations ($\Delta T = 0.267 \text{ ps}$), the fidelity curve produced exactly overlaps with that of the solid blue line of Figure 3.

2. NOT₂ quantum gate

The total pulse energy was kept constant at $E = 20 \mu\text{J}$ and with $n = 2$ the two transition frequencies were $\nu_1 = 2121 \text{ cm}^{-1}$ and $\nu_2 = 2151 \text{ cm}^{-1}$, with the central frequency being $\nu_0 = 2136 \text{ cm}^{-1}$. Binary laser pulses ($2A/2\phi$) were implemented. Using the notation $[A_1\phi_1, A_2\phi_2]$, with subscripts referring to either transition frequency, a total of $(2 \times 2)^2 = 16$ laser pulse combinations result. Only 9 of the combinations are unique and one of the nine combinations is the field free case; thus only 8 combinations were calculated. The resulting fidelities for the 8 unique laser pulse combinations for each value of T are shown in Figure 4. It is important to note that

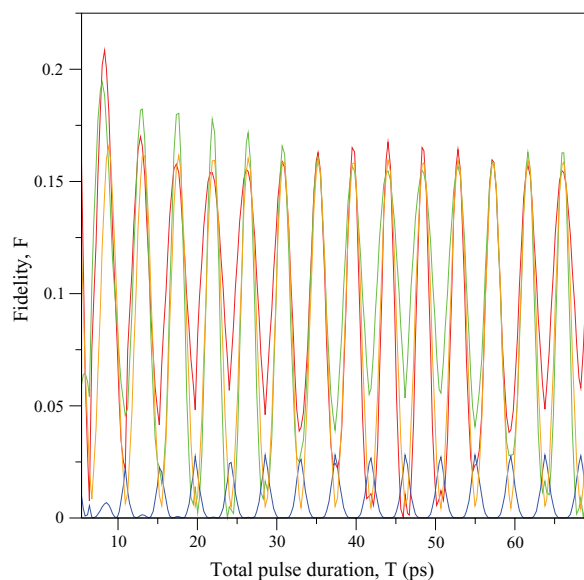


FIG. 4. Plot of the resulting fidelities for eight pulse shapes (only 4 are unique) as a function of the total pulse duration T for the NOT₂ quantum gate having a total pulse energy of $20 \mu\text{J}$. The laser pulses, consisting of two frequency components ($n = 2$) at the transition frequencies ($\nu_1 = 2121 \text{ cm}^{-1}$, $\nu_2 = 2151 \text{ cm}^{-1}$) with binary pulse shaping ($2A/2\phi$) using the notation $[A_1\phi_1, A_2\phi_2]$, are $[1\pi, 1\pi] = [10, 10]$ red line, $[10, 1\pi] = [1\pi, 10]$ green line, $[1\pi, 00] = [10, 00]$ blue line, and $[00, 1\pi] = [00, 10]$ orange line.

the plots in Figure 4 have considerably lower fidelities due to inappropriate choice of total laser pulse energy and insufficient amplitude variation beyond 2 amplitude components ($2A$). Some of the laser pulse combinations produce identical dynamics in Figure 4, namely, $F_{[1\pi, 1\pi]} = F_{[10, 10]}$ (red line), $F_{[10, 1\pi]} = F_{[1\pi, 10]}$ (green line), $F_{[1\pi, 00]} = F_{[10, 00]}$ (blue line), and $F_{[00, 1\pi]} = F_{[00, 10]}$ (orange line). The red, green, and orange lines in Figure 4 seem to oscillate at approximately the same frequency while the blue line seems to be centered at their minima but with a much lower fidelity. Finally, Sec. III B will show that high fidelity points do not necessarily mean 100% fidelity points.

3. Had₂ quantum gate

The total pulse energy was kept constant at $E = 25 \mu\text{J}$. Similarly to the NOT₂ gate, there are only 8 unique laser pulse combinations using 2 frequency components $\nu_1 = 2121 \text{ cm}^{-1}$ and $\nu_2 = 2151 \text{ cm}^{-1}$, centered at $\nu_0 = 2136 \text{ cm}^{-1}$. The results are shown in Figure 5. We refer the reader to the ACNOT₁ results shown in the inset of Figure 3, illustrating the fluctuating fidelities between pulse shapes differing in phase by π . Similar fidelity trends are observed for the results from specific laser pulse amplitude and phase combinations for the Had₂ quantum gate. Fidelity results of all pulse combinations for ACNOT₁ are plotted in Figure 3. However, in the case of Figure 5 for the Had₂ gate, in order to simplify the figure the fluctuations are not shown. Only the maximum fidelities between the following combinations are plotted, namely $[1\pi, 1\pi]$ and $[10, 10]$ (red line), $[10, 1\pi]$ and $[1\pi, 10]$ (green line), $[1\pi, 00]$ and $[10, 00]$ (blue line), and $[00, 1\pi]$ and $[00, 10]$ (orange line). The black line of Figure 5(e) displays the maximum fidelity between either four possible values of Figs. 5(a)–5(d), at any given total pulse duration. The curves are more com-

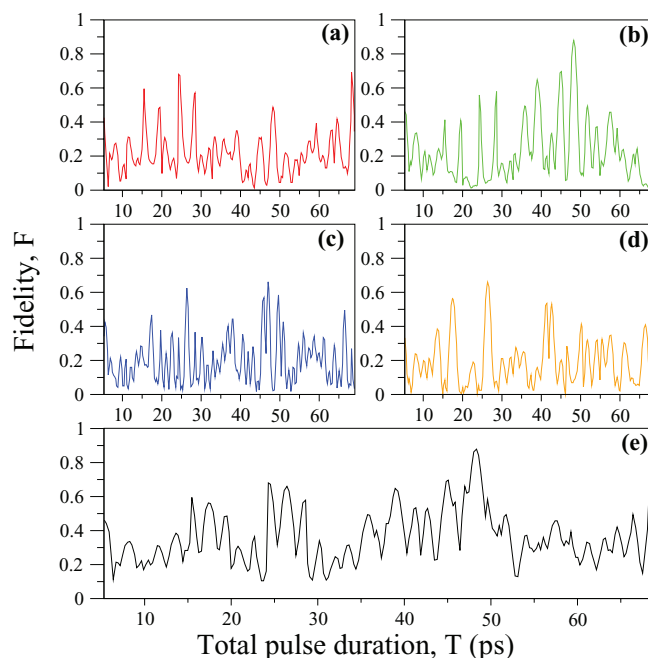


FIG. 5. Plot of the resulting maximum fidelities for 8 pulse shapes as a function of the total pulse duration T for the Had₂ quantum gate having a total pulse energy of $25 \mu\text{J}$. The laser pulses, consist of 2 frequency components ($n = 2$) at the transition frequencies ($\nu_1 = 2121 \text{ cm}^{-1}$, $\nu_2 = 2151 \text{ cm}^{-1}$) with binary pulse shaping ($2A/2\phi$) using the notation $[A_1\phi_1, A_2\phi_2]$, are (a) $[1\pi, 1\pi]$ and $[10, 10]$ red line, (b) $[10, 1\pi]$ and $[1\pi, 10]$ green line, (c) $[1\pi, 00]$ and $[10, 00]$ blue line, and (d) $[00, 1\pi]$ and $[00, 10]$ orange line. Also plotted, in black within (e), are the maximum results from the previous plots of (a)–(d), at any given total pulse duration.

plicated than those obtained for the ACNOT₁ or NOT₂ gates, likely due to the required superposition of states of the Had₂ gate. In this case there is no regular pattern, making it difficult to deduce a predictable value of T that will result in a high fidelity.

B. Effect of laser pulse energy (F vs. A)

As a first attempt to improve upon the fidelity, the optimal laser pulse energy was determined at select total pulse durations, T . These calculations could have been done for every value of T in Sec. III A and would have provided a more complete picture but the optimization time requirements limited this. Using $n = 1$ for the ACNOT₁ gate or $n = 2$ for the NOT₂ and Had₂ gates, we varied the amplitude from $2A$ choices of amplitude, up to a maximum of $512A$ amplitude choices, while restricting the phase to 2ϕ choices, $\phi = 0$ or π . For example, the designation $512A$ can be thought of as dividing up the amplitude, at each frequency discretization, into a maximum of 512 segments. Moreover, by varying the amplitude what is actually being optimized is the energy associated with each frequency component used in the calculation. Thus, the actual laser pulse energy reported will be much less than the total pulse energy since only a small fraction of the total pulse energy is carried in the discretized frequency component(s) used here. The laser pulse energy was increased to a value larger than used in Sec. III A, in order to allow more flexibility in the choice of energy. For the ACNOT₁ gate an energy of $30 \mu\text{J}$ was used. For the NOT₂ and Had₂ gates, since

TABLE II. Comparison of resulting fidelities, pulse energies, and amplitudes for laser pulses optimized for the ACNOT₁ gate with and without (optimal) amplitude restrictions. The amplitude used in Figure 3 is $A = 1.00$ and the total pulse energy was $30 \mu\text{J}$.

Total pulse duration T (ps)	Figure 3 fidelity F	Optimal fidelity F	Figure 3 pulse energy E (μJ)	Optimal pulse energy E (μJ)	Optimal amplitude A
7.47	0.9747	0.9748	0.8388	0.8519	0.339
11.20	0.2712	0.2715	0.5592	0.5351	0.319
22.68	0.5049	0.5058	0.2763	0.2953	0.356
45.10	0.5660	0.5680	0.1390	0.1248	0.299

two frequencies are needed that are not at the central peak intensity (see Figure 2), a value of $100 \mu\text{J}$ is used. In general, optimizing the energy did not change the relative relationship between low and high fidelity points in Figs. 3–5.

1. ACNOT₁ quantum gate

Values for the total pulse duration associated with high and low fidelities were chosen from Figure 3, namely, 7.47 ps, 11.20 ps, 22.68 ps, and 45.10 ps. The results comparing a total laser pulse energy of $10 \mu\text{J}$ with an optimized laser pulse energy chosen from a total pulse energy of $E = 30 \mu\text{J}$ for 512A, are displayed in Table II. In this case the chosen value of $E = 10 \mu\text{J}$ for all 4 cases, when using $2A$ and 2ϕ components, was able to produce the required optimal pulse energy. With a choice of 7.47 ps pulse duration and using only one frequency component at the transition frequency, a $30 \mu\text{J}$ total laser pulse energy could produce a high fidelity (here $F = 0.9748$) when using 512A amplitude variations.

The pulse durations 22.68 ps and 45.10 ps correspond to local maxima of Figure 3. Analysis of the fidelity at these two points indicate that there is poor phase alignment between the qubits. For example, the optimal laser pulse in Table II at 45.10 ps produces resultant qubit phases of: $\Phi_{|00\rangle} = -1.50$ rad, $\Phi_{|01\rangle} = -1.50$ rad, $\Phi_{|10\rangle} = -0.09$ rad, and $\Phi_{|11\rangle} = -0.04$ rad. It is this lack of phase alignment that produces the unexpectedly low fidelity at $T = 22.68$ ps and 45.10 ps. In comparison, analogous data for the high fidelity pulse duration $T = 7.47$ ps is $\Phi_{|00\rangle} = -1.99$ rad, $\Phi_{|01\rangle} = -1.99$ rad, $\Phi_{|10\rangle} = -2.33$ rad, and $\Phi_{|11\rangle} = -2.25$ rad. The resulting phases of the qubits involved in the transition, $|00\rangle$ and $|01\rangle$, are the same because the laser pulse is symmetric (see Sec. II C).

2. NOT₂ quantum gate

Values for the total pulse duration at four high fidelity points 8.27 ps, 35.22 ps, 44.03 ps, 52.84 ps, and one low fidelity point 15.21 ps were chosen from Figure 4. The results comparing a constant laser pulse energy of $20 \mu\text{J}$ for $2A$ amplitude variations with an optimized laser pulse energy at a maximum $E = 100 \mu\text{J}$ for 512A amplitude variations, are displayed in Table III. The initial choice of $E = 20 \mu\text{J}$ with $2A$ amplitude variations produces very low fidelities (Table III; Figure 3 fidelity). Once the amplitudes were given more variation (512A) under a larger energy window ($100 \mu\text{J}$), the fidelities increased dramatically (Table III; Optimal fidelity).

TABLE III. Comparison of resulting fidelities, pulse energies, and amplitudes for laser pulses optimized for the NOT₂ gate with and without (optimal) amplitude restrictions. The amplitudes, A_1/A_2 , for Figure 4 are 1.00/1.00 and the total pulse energy was $100 \mu\text{J}$.

Total pulse duration T (ps)	Figure 4 fidelity F	Optimal fidelity F	Figure 4 pulse energy E (μJ)	Optimal pulse energy E (μJ)	Optimal amplitudes A_1/A_2
8.27	0.2085	0.7461	2.820	7.297	0.035/1.00
15.21	0.0414	0.4256	1.571	5.203	0.376/0.949
35.22	0.1629	0.7372	0.668	1.679	0.049/0.957
44.03	0.1675	0.9994	0.534	1.281	0.051/0.908
52.84	0.1641	0.8459	0.445	0.621	0.458/0.010

Larger pulse energies were required in order to obtain larger fidelities. According to Table III, a low amplitude at one of the two frequencies and a high amplitude at the other is needed to achieve optimal fidelities at a given value of T , for $n = 2$. For example optimizing the laser pulse energy for a total pulse duration of $T = 8.27$ ps, results in an optimal amplitude of $A_1 = 0.035$ and $A_2 = 1.00$ for ν_1 and ν_2 , respectively. With reference to Eq. (3), the laser pulse with a frequency of $\nu_1 = 2121 \text{ cm}^{-1}$ has a low amplitude A_1 than the $\nu_2 = 2151 \text{ cm}^{-1}$ laser pulse with $A_2 = 1.00$. These choices of amplitudes result in high fidelities which would not have been achieved by a constant laser pulse energy with binary pulse shaping (Figure 4).

3. Had₂ quantum gate

For the case of the ACNOT₁ and NOT₂ quantum gates, the choice of T at high and low fidelity points from Figure 3 or Figure 4 lead to a fairly simple regular structure. The analogous plot for the Had₂ gate (Figure 5) is very complex in structure, exhibiting no signs of a regular pattern. Only two total pulse durations with high fidelity points were studied from Figure 5, namely, 24.28 ps and 48.30 ps. The results comparing a constant laser pulse energy of $25 \mu\text{J}$ with an optimized laser pulse energy at a maximum energy of $100 \mu\text{J}$ for 512A amplitude variations, are displayed in Table IV. The constant $25 \mu\text{J}$ laser pulse energy was not optimal, as seen by the large discrepancy between the fidelities. The fidelity can be significantly improved by changing the pulse energy, e.g., the laser pulse optimized at $T = 48.30$ ps attains a large fidelity ($F = 0.9742$). The choice of optimal amplitudes is different in this case than for the NOT₂ gate since A_1 and A_2 are of similar magnitudes.

TABLE IV. Comparison of resulting fidelities, pulse energies, and amplitudes for laser pulses optimized for the Had₂ gate with and without (optimal) amplitude restrictions. The amplitudes, A_1/A_2 , for Figure 5 are 1.00/1.00 and the total pulse energy was $30 \mu\text{J}$.

Total pulse duration T (ps)	Figure 5 fidelity F	Optimal fidelity F	Figure 5 pulse energy E (μJ)	Optimal pulse energy E (μJ)	Optimal amplitudes A_1/A_2
24.28	0.6810	0.8817	1.197	1.199	0.344/0.157
48.30	0.8791	0.9742	0.609	0.660	0.315/0.227

TABLE V. Results of amplitude (A), phase (ϕ), and number of frequency components (n) variation at select pulse durations from Sec. III B for the ACNOT₁, NOT₂, and Had₂ quantum gates. Also included are results from full calculations (*full*) in which the amplitude at each frequency was flexible to vary by 32 segments between $0 \leq A \leq 1$.

n	A/ϕ	ACNOT ₁ $T = 7.47$ $A_1 = 0.339$		NOT ₂ $T = 52.84$ $A_1/A_2 = 0.458/0.010$		Had ₂ $T = 24.28$ $A_1/A_2 = 0.344/0.157$	
		Fidelity	Avg. pop.	Fidelity	Avg. pop.	Fidelity	Avg. pop.
1 or 2	$2A/2\phi$	0.9748	0.9983	0.8459	0.9955	0.8817	0.9068
	$2A/32\phi$	0.9748	0.9983	0.8459	0.9955	0.8817	0.9068
13 or 10	$2A/2\phi$	0.9876	0.9947	0.8921	0.9427	0.8817	0.9068
	$32A/2\phi$	0.9912	0.9956	0.9123	0.9726	0.9834	0.9873
	$2A/32\phi$	0.9880	0.9949	0.9067	0.9683	0.8817	0.9068
<i>Full</i> 13 or 10	$32A/2\phi$	0.9927	0.9948	0.9638	0.9875	0.9840	0.9847

C. Effect of number of frequency components, amplitude, and phase (F vs. n , A , ϕ)

From Secs. III A and III B, it is clear that the overall quantum gate fidelity is strongly dictated by the one (ACNOT₁) or two (NOT₂ and Had₂) transition frequency components. Here we want to consider what role additional frequency components play in determining the overall fidelity and subsequent amplitude and phase variation on these additional frequencies. In order to do so, one of the values of the total pulse duration (T) from Sec. III B for each quantum logic gate must be selected. The optimal amplitude(s) determined for this choice of pulse duration are then used as the maximum values instead of the default of 1.00. The result is an optimal amplitude (energy) at each transition frequency from which to vary the amplitude (A) and/or phase (ϕ) for increasing number of frequency components (n). For the ACNOT₁ gate the number of frequency components varies by odd integer values according to $1 \leq n \leq 13$, so that frequency components are added to either side of the transition frequency. The NOT₂ and Had₂ gates vary by $n = 2, 6$, and 10, so that frequency components are added to either side of both transition frequencies (see Sec. II C and Figure 2). Combinations of $2A$ or $32A$ and 2ϕ or 32ϕ for each number of frequency components were used to test the effect of increased amplitude or phase variation on the optimal fidelity. Also an optimization in which the energy had $32A$ amplitude variations and the phase with 2ϕ variation at each value of $n = 10$ or 13 frequency components was used as a comparison—here termed the *full* optimization. In this *full* optimization there was no determined optimal amplitude and the default maximum amplitude ($A = 1.00$) was used for all frequencies, thus giving more flexibility for the allowed energies. This is analogous to the energy optimization of Sec. III B, except in this case $n = 10$ or $n = 13$ and results in a very large parameter space optimization. The results for the minimum and maximum number of frequency components studied are shown in Table V. In our previous study, we also produced GA optimized laser pulses for the ACNOT₁, NOT₂, and Had₂ gates but using binary pulse shaping for $n = 51$ frequency components at $T = 6.67$ ps.³² Fidelities of $F_{ACNOT_1} = 0.9729$, $F_{NOT_2} = 0.5118$, and $F_{Had_2} = 0.5075$ were obtained using a total pulse energy of 10 μJ , 20 μJ , and 25 μJ , respectively.

1. Effect of amplitude - A

As was shown in Sec. III B, the use of amplitude variance allowed for laser pulse energy optimization. This produced a very large increase in the fidelity, in many instances. When $32A/2\phi$ with $n = 13$ was used, the fidelity for the ACNOT₁ gate rose subtly from 0.9876 ($2A/2\phi$) up to $F = 0.9912$. In the case of the Had₂ gate with $2A/2\phi$, restricting the maximum amplitudes to $A_1 = 0.344$ and $A_2 = 0.157$ limited the fidelity from increasing (constant $F = 0.8817$) even when the number of frequency components was increased to $n = 13$. When either $n = 2$ or when $n = 13$, the same laser pulse shape, consisting of only the transition frequencies, was chosen. Giving flexibility to the amplitudes ($32A/2\phi$, $n = 13$) of the Had₂ gate allowed the fidelity to increase to 0.9834, which is very close to the full optimization fidelity of 0.9840. For the NOT₂ gate with $n = 13$ using $32A/2\phi$, the fidelity of the optimal laser pulse, $F = 0.9132$, is significantly less than the full optimization of 0.9638. In this case there are energies at specific frequencies that are greater than the maximum allowed by the amplitude restriction of $A_1 = 0.458$ or $A_2 = 0.010$. Increasing the amplitude variance while using these maximum values will not improve the fidelity to that of the full optimization value.

2. Effect of phase - ϕ

The increase of phase, beyond $\phi = 0$ or π , to 32ϕ has minimal effect (increase of 1.5%) or no effect on increasing the fidelity. The necessary phase condition is that the parameter space at least consists of $\phi = 0$ to produce positive amplitudes and $\phi = \pi$ in order to produce negative amplitudes (see Eq. (3)). An optimization for the ACNOT₁ gate with $n = 13$ using $2A/2\phi$ produces $F = 0.9876$, while a choice of $2A/32\phi$ gives a minor increase to $F = 0.9880$. The population transfers between the qubits for both cases are shown in Figure 6, along with the amplitude and phase sequence at $\nu_0 = 2151 \text{ cm}^{-1}$.

3. Effect of number of frequency components - n

The effect of adding additional frequency components is dependent upon the ability for the amplitude and/or phase to

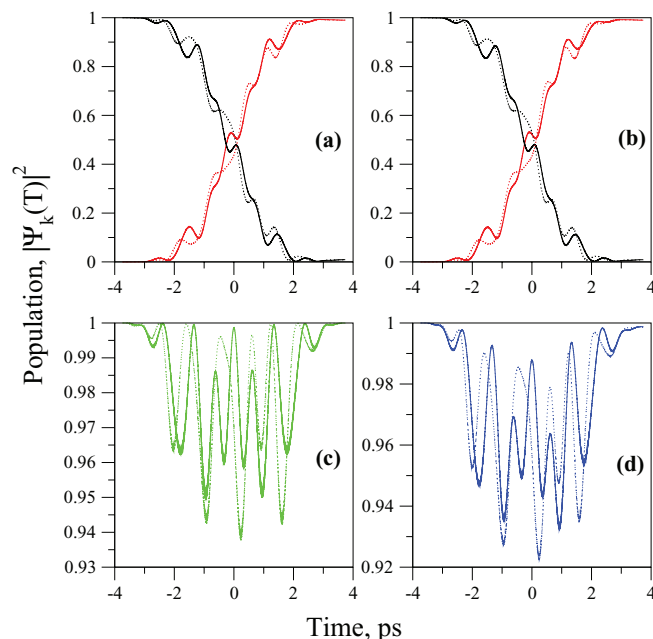


FIG. 6. Plot of the population dynamics between qubits for the ACNOT₁ gate using $n = 13$ frequency components with a total pulse energy of 30 μJ for $2A/2\phi$ (solid line) and for $2A/32\phi$ (dotted line). (a) $|00\rangle \rightarrow |01\rangle$, (b) $|01\rangle \rightarrow |00\rangle$, (c) $|10\rangle \rightarrow |10\rangle$, and (d) $|11\rangle \rightarrow |11\rangle$. Black: $|00\rangle$, red: $|01\rangle$, green: $|10\rangle$, and blue: $|11\rangle$. The sequence of laser pulse amplitudes and phases $[A_1\phi_1, \dots, A_{13}\phi_{13}]$, with a central frequency of $\nu_0 = 2151 \text{ cm}^{-1}$, that produce the solid lines are $[00,00,00,00,00,00,0.339\pi,00,00,0.339\pi,0.339\pi,0.339\pi,0.339\pi]$ and the dotted lines are $[00,00,00,00,00,00,0.339\pi,00,00,0.339\pi,0.339\pi,0.339\pi,0.339\pi]$.

increase the fidelity. The addition of further frequency components beyond the transition frequency/frequencies causes a small increase in fidelity; the majority of the fidelity coming from the transition frequency/frequencies themselves. The former statement occurs for the Had₂ gate in which the fidelity has reached a maximum of 0.8817 and no further increase is accomplished by increasing the number of frequency components. The fidelity increases to 0.9834 once the amplitudes are allowed more flexibility by using 32A amplitude variations. The latter can be noted for the ACNOT₁ gate in which an already high fidelity ($F = 0.9748$) when using only $n = 1$ at the transition frequency and $2A/2\phi$, increases in fidelity only moderately when the number of frequency components is increased.

D. Qubit population dynamics

To illustrate the nature of the qubit excitations, the population dynamics for selected quantum gates are plotted. For the ACNOT₁ gate there is a comparison between the $T = 7.47 \text{ ps}$ single frequency using $n = 1$ with $2A/2\phi$ optimization ($F = 0.9748$) and to the full $T = 7.47 \text{ ps}$ using $n = 13$ with $32A/2\phi$ optimization ($F = 0.9927$). The comparison for the NOT₂ gate is between two high fidelity points for different pulse durations, namely, 44.03 ps using $n = 1$ with $2A/2\phi$ optimization ($F = 0.9994$) and 52.84 ps using $n = 10$ with $32A/2\phi$ optimization ($F = 0.9123$). Finally, a comparison is made between the Had₂ gate when $T = 24.28 \text{ ps}$ using

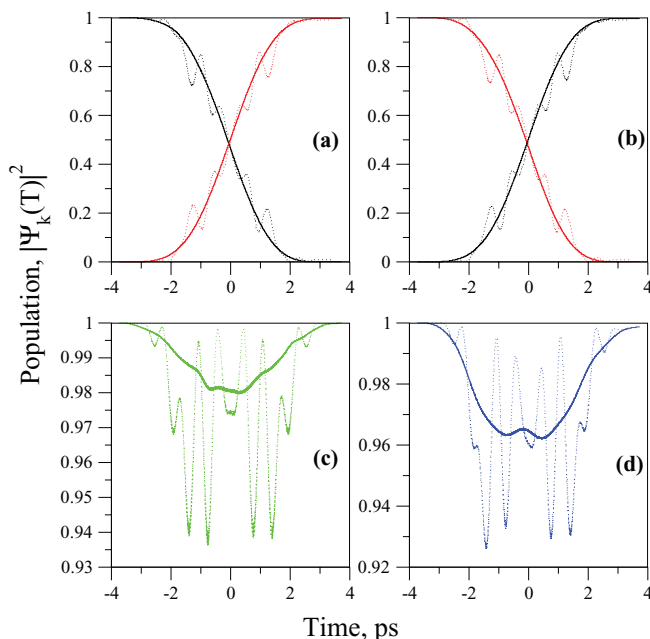


FIG. 7. Resulting population dynamics for the four qubit transformations of the ACNOT₁ quantum gate of pulse duration $T = 7.47 \text{ ps}$ when using $n = 1$ with $2A/2\phi$ (solid lines) and using $n = 13$ with $32A/2\phi$ (dotted lines). (a) $|00\rangle \rightarrow |01\rangle$, (b) $|01\rangle \rightarrow |00\rangle$, (c) $|10\rangle \rightarrow |10\rangle$, and (d) $|11\rangle \rightarrow |11\rangle$. Black: $|00\rangle$, red: $|01\rangle$, green: $|10\rangle$, and blue: $|11\rangle$.

$n = 10$ with $32A/2\phi$ ($F = 0.9834$) and $T = 48.30 \text{ ps}$ using $n = 1$ with $2A/2\phi$ ($F = 0.9742$).

1. ACNOT₁ quantum gate

Figure 7 illustrates the resulting population dynamics for laser pulses optimized using $T = 7.47 \text{ ps}$ with the single transition frequency 2151 cm^{-1} ($n = 1$) and $2A/2\phi$ components, and also $T = 7.47 \text{ ps}$ at 2151 cm^{-1} but with multiple frequency components ($n = 13$) and $32A/2\phi$. In Figures 7(a) and 7(b) the qubit transition $|00\rangle \leftrightarrow |01\rangle$ (black and red, respectively) is shown. A pulse area theorem analysis^{42–45} of the resulting laser pulse and corresponding transition dipole moment using a single frequency laser pulse ($n = 1$; Figure 7, solid line) coincides well with the resulting population dynamics. Using Eq. (9) from the work of Cheng and Brown,⁴⁵ for determining the pulse area, produces a value of 1.04π . This result corresponds to the first occurrence of population inversion between the two qubits which is observed as a $\frac{1}{2}$ Rabi cycle. When a laser pulse optimization is carried out for $n = 13$ (solid line) the population dynamics seem to be a more complicated form of $\frac{1}{2}$ Rabi cycle. For the $|10\rangle \rightarrow |10\rangle$ (Figure 7(c)) and $|11\rangle \rightarrow |11\rangle$ (Figure 7(d)) qubit transitions, requiring only a phase change to ensure global phase alignment, there is a small amount of intermediate population exchange between nearby qubits. Specifically, in both cases, a small exchange was observed for qubit $|10\rangle$ with $|11\rangle$ and $|10\rangle$, and $|11\rangle$ with $|01\rangle$ and $|10\rangle$. The majority of the fidelity for the ACNOT₁ gate under these conditions is attributed to the central frequency and optimal pulse energy. Further fidelity increases are attributed to variations in frequency components and amplitude, in order to bring the fidelity near 100%.

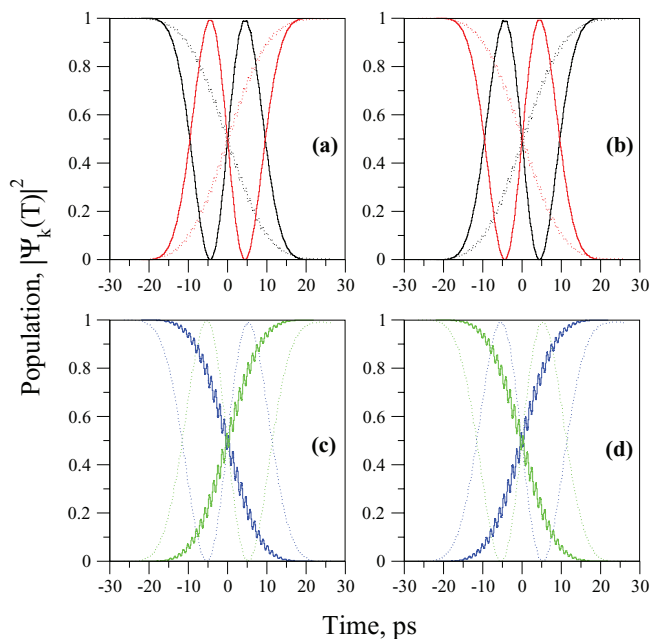


FIG. 8. Resulting population dynamics for the four qubit transformations of the NOT₂ quantum gate when using a pulse of length $T = 44.03$ ps, $n = 1$, and $2A/2\phi$ (solid lines), and using a pulse of length $T = 52.84$ ps, $n = 10$, and $32A/2\phi$ (dotted lines). (a) $|00\rangle \rightarrow |01\rangle$, (b) $|01\rangle \rightarrow |00\rangle$, (c) $|10\rangle \rightarrow |11\rangle$, and (d) $|11\rangle \rightarrow |10\rangle$. Black: $|00\rangle$, red: $|01\rangle$, green: $|10\rangle$, and blue: $|11\rangle$.

2. NOT₂ quantum gate

The population dynamics for optimized laser pulses with $T = 44.03$ ps using $n = 1$ with $2A/2\phi$ and an optimized laser pulse with $T = 52.84$ ps using $n = 10$ with $32A/2\phi$ are shown in Figure 8. Figures 8(a) and 8(b) illustrate that for $T = 44.03$ (solid line) the $|00\rangle \leftrightarrow |01\rangle$ transition proceeds through a $\frac{3}{2}$ Rabi cycle and the $|10\rangle \leftrightarrow |11\rangle$ transition through a $\frac{1}{2}$ Rabi cycle. This observation is also concluded by a pulse area theorem analysis of the laser pulse and respective transition dipole moments, as implemented previously for ACNOT₁. By using the analytic form of the laser field (Eq. (3)) the sub-pulses constituting each individual resonant transition can be determined. The sub-pulse with frequency and transition dipole moment corresponding to the $|00\rangle \leftrightarrow |01\rangle$ transition produces a value of 3.008π whereas similar pulse area theorem analysis for the $|10\rangle \leftrightarrow |11\rangle$ transition produces a value of 1.005π . The value of 3.008π corresponds to the second occurrence of population inversion or observed $\frac{3}{2}$ Rabi cycle and the value of 1.005π corresponds to the first occurrence of population inversion or $\frac{1}{2}$ Rabi cycle. The Rabi cycle pathways are switched when the total pulse duration is $T = 52.84$. It is also possible to enforce the transitions to be both $\frac{1}{2}$ Rabi cycles. For $T = 52.84$ ps, $n = 2$, and $E = 100 \mu\text{J}$, the initial maximum amplitudes were selected as: $A_1 = 0.125$ ($64A$, 2ϕ) and $A_2 = 1.00$ ($512A$, 2ϕ). The amplitude restriction is enforced on A_1 since we know from Table V the optimal value for A_2 will be low (0.010). The anticipated $\frac{1}{2}$ Rabi cycle was produced for both NOT₂ gate transitions and resulted in $A_1 = 0.0516$, $A_2 = 0.098$, and $F = 0.8024$. A larger fidelity was found when A_1 was not restricted ($F = 0.8459$; Table V) and thus the transitions which both consist of $\frac{1}{2}$ Rabi cycles were not optimally chosen by the GA.

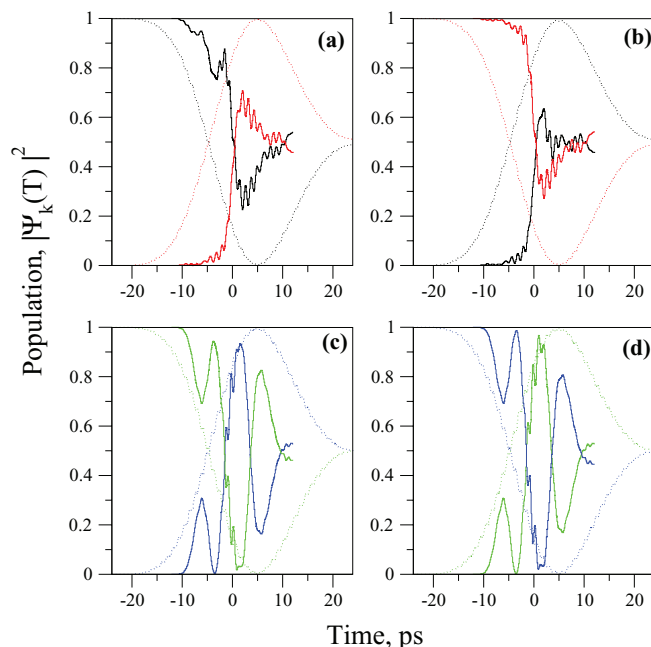


FIG. 9. Resulting population dynamics for the four qubit transformations of the Had₂ quantum gate when using a pulse of length $T = 24.28$ ps, $n = 10$, and $32A/2\phi$ (solid lines), and using a pulse of length $T = 48.30$ ps, $n = 1$, and $2A/2\phi$ (dotted lines). (a) $|00\rangle \leftrightarrow \frac{1}{\sqrt{2}}(|00\rangle + |01\rangle)$, (b) $|01\rangle \leftrightarrow \frac{1}{\sqrt{2}}(|00\rangle - |01\rangle)$, (c) $|10\rangle \leftrightarrow \frac{1}{\sqrt{2}}(|10\rangle + |11\rangle)$, and (d) $|11\rangle \leftrightarrow \frac{1}{\sqrt{2}}(|10\rangle - |11\rangle)$. Black: $|00\rangle$, red: $|01\rangle$, green: $|10\rangle$, and blue: $|11\rangle$.

3. Had₂ quantum gate

Finally, the population dynamics for optimized laser pulses with $T = 24.28$ ps using $n = 10$ with $32A/2\phi$ and $T = 48.30$ ps using $n = 1$ with $2A/2\phi$ are shown in Figure 9. This figure illustrates that the $T = 48.30$ ps optimized laser pulse causes all qubit transitions to proceed through a $\frac{3}{4}$ Rabi cycle. This is verified with a subsequent pulse area theorem analysis, analogous to those carried out with the NOT₂ gate above. The transitions involving the qubits $|00\rangle$ and $|01\rangle$ produce a value of 1.493π , and those involving $|10\rangle$ and $|11\rangle$ produce a value of 1.496π . When the laser pulse optimized is 24.28 ps, the resulting optimized laser pulse produces relatively complex population dynamics, requiring many intermediate exchanges of population between qubit pairs and other rovibrational states of the Had₂ gate. This being attributed to having more frequency components ($n = 10$).

IV. CONCLUSION

A number of experimental pulse shaping parameters and their effects on the fidelities of laser pulses shaped to represent the ACNOT₁, NOT₂, and Had₂ quantum logic gates, were studied. Pulse shaping occurs in the frequency domain using a discretized spectrum with independent control of amplitude and phase dependent frequencies, similar to current LC-SLM setups. The parameters that were varied are (i) the frequency resolution ($d\nu$) or synonymously the pulse duration (T), (ii) the number of frequency components (n), (iii) the number of amplitude components (A_j), and (iv) the number of phase components (ϕ_j). A time domain analytic

form for the discretized frequency spectrum was also formulated.

Initially, an exploration of the pulse duration was carried out for each quantum gate using laser pulses with with $2A$ and 2ϕ variation of $A = 0$ or 1 and $\phi = 0$ or π . The resulting plots showed a simple relationship between the fidelity and pulse duration for the ACNOT₁ and NOT₂ gates. The plot obtained for the Had₂ gate showed a complex relationship. The trends observed for the ACNOT₁ gate fidelities at chosen pulse durations was attributed to the difference in the natural evolution of the rovibrational state qubits $|10\rangle$ and $|11\rangle$.

In order to determine the optimal laser pulse energy at the qubit transition frequency/frequencies for each quantum logic gate shaped laser pulse, the amplitudes were varied by $512A$, while keeping the phase at 2ϕ (0 or π), for select values of pulse duration. The optimal amplitude chosen for each pulse duration at $30 \mu\text{J}$ for the ACNOT₁ gate was already very near the previous choice of 1.0 for a $10 \mu\text{J}$ pulse, so the fidelities did not change substantially. Two transition frequencies were required for the NOT₂ and Had₂ gates, and the resulting amplitudes were of differing magnitudes indicating that one transition requires more energy than the other. A substantial increase in the fidelity was observed in these cases since the previous optimizations used non-optimal laser pulse energies.

Finally, we investigated the affect of increasing the number of frequency components on quantum gate fidelities. Laser pulses of one pulse duration each were shaped with 13 frequencies (ACNOT₁) or 10 frequencies (NOT₂ and Had₂) each with $2A/2\phi$, $32A/2\phi$, and $2A/32\phi$ amplitude and phase combinations. A *full* optimization of 13 or 10 frequencies and $32A/2\phi$ was calculated, but without optimizing the transition frequency energy and allowing the amplitudes to have more energy flexibility per frequency component. Again, amplitude variation played a major role in improving the fidelities and in some cases caused an improvement of 10%. Surprisingly, phase variation at most caused an increase of only 1.5%. The *full* optimization was very close to the results of regular $32A/2\phi$ variation, except in the case of the NOT₂ gate, likely due to the necessity of large variations in energy per frequency component.

Overall, it was determined that the majority of the quantum gate fidelity resides in the transition frequency/frequencies and more so determining an optimal energy associated with them. Addition of further frequency components can cause some incremental increases in the fidelity. Moreover, optimized laser pulses that produce large fidelities exhibit pulse areas that obey optimal pulse area theorem solutions. For the case of the ACNOT₁ and NOT₂ quantum gates when $n = 1$ or 2 , respectively, optimally shaped laser pulses produce values of odd integer multiples of π (e.g., π , 3π) in order to induce recurring population inversions. High fidelity optimally shaped laser pulses for the Had₂ quantum gate when $n = 2$ produce values of odd half integer multiples of π (e.g., $\frac{3\pi}{2}$) in order to induce recurring superpositions between the qubits. Also, the variation of phase seemed to provide no significant improvement upon the fidelity. High fidelity control of rovibrational state qubits for quantum gate operation through a shaped laser pulse also

seems to be largely influenced by the natural evolution of the qubits.

As mentioned in the introduction, OCT is another commonly implemented laser pulse optimization procedure. It is difficult to compare and contrast results obtained by OCT versus those by the GA because the OCT algorithm would require discrete frequency filtering to resemble the GA model. Moreover, the method by which global phase alignment is implemented within OCT is different than the fidelity function used in GA optimizations and thus so is the weight of global phase alignment in each. Subsequent optimizations by OCT and GA would have differing selective pressures and, in general, would end up in differing regions of the laser pulse search space. In our previous study³¹ we used OCT and GA procedures together to show that optimal laser pulses can be shaped in either case but comparisons between the results of each could not be clearly made. It may be necessary from a theoretical stand point that further investigations be done in order to elucidate relationships between laser pulses shaped using OCT and GA optimizations, and the resulting dynamics.

ACKNOWLEDGMENTS

The authors thank the Natural Sciences and Engineering Research Council of Canada (NSERC Discovery Grant) for financial support. We thank the Canadian Foundation for Innovation (New Opportunities Fund) for support of the computational infrastructure on which this work was carried out. R.R.Z. appreciates the Natural Sciences and Engineering Research Council of Canada (NSERC) for financial support through the PGS-D2 scholarship.

APPENDIX: DERIVATION OF THE ANALYTIC FORM OF THE LASER PULSE

We begin the derivation of an analytic form of the laser pulse, by starting with the simple condition of the discretized frequency domain laser pulse, $f(\nu)$, consisting of a single frequency component centered at ν_j with a resolution, $d\nu$,

$$f(\nu) = \begin{cases} \epsilon(\nu_j), & \nu_j - \frac{d\nu}{2} \leq \nu \leq \nu_j + \frac{d\nu}{2} \\ 0 & \text{otherwise} \end{cases} \quad (\text{A1})$$

Since there is only one frequency component, everywhere else outside of the frequency resolution is satisfied by $f(\nu) = 0$. This would be the condition of Figure 2(a) if only the central frequency, ν_0 , were considered. A Fourier transform of this frequency domain laser pulse $f(\nu)$, produces the resulting time domain laser pulse, $F(t)$,

$$F(t) = \int_{\nu_j - \frac{d\nu}{2}}^{\nu_j + \frac{d\nu}{2}} f(\nu) e^{i2\pi\nu t} d\nu. \quad (\text{A2})$$

Substituting in the Fourier transform, our initial case of a single frequency laser pulse, produces the following:

$$\begin{aligned} F(t) &= \epsilon(v_j) \int_{v_j - \frac{\Delta v}{2}}^{v_j + \frac{\Delta v}{2}} e^{i2\pi vt} dv \\ &= \epsilon(v_j) \left(\frac{e^{i2\pi t dv/2} - e^{-i2\pi t dv/2}}{i2\pi t} \right) e^{i2\pi v_j t} \\ &= \epsilon(v_j) \frac{\sin(\pi t dv)}{\pi t} e^{i2\pi v_j t}. \end{aligned} \quad (\text{A3})$$

The resulting equation can be written in terms of a sinc function,

$$F(t) = dv\epsilon(v_j) \text{sinc}(\pi t dv) e^{i2\pi v_j t}, \quad \text{sinc}(x) = \frac{\sin(x)}{x}. \quad (\text{A4})$$

Substituting explicitly the frequency domain laser pulse intensity, $\epsilon(v_j)$, used in this case, one obtains

$$\begin{aligned} F(t) &= dv\epsilon_0 \sqrt{A_j} e^{-2\ln 2 \left(\frac{v_j - v_0}{\Delta v} \right)^2} e^{i\phi_j} \text{sinc}(\pi t dv) e^{i2\pi v_j t} \\ &= dv\epsilon_0 \sqrt{A_j} e^{-2\ln 2 \left(\frac{v_j - v_0}{\Delta v} \right)^2} \text{sinc}(\pi t dv) e^{i(2\pi v_j t + \phi_j)}. \end{aligned} \quad (\text{A5})$$

The laser pulse is a real quantity, such that

$$\begin{aligned} \Re [F(t)] &= dv\epsilon_0 \sqrt{A_j} e^{-2\ln 2 \left(\frac{v_j - v_0}{\Delta v} \right)^2} \text{sinc}(\pi t dv) \cos(2\pi v_j t + \phi_j). \end{aligned} \quad (\text{A6})$$

The resulting single frequency laser pulse produced from a discretized frequency spectrum is

$$\Re [F(t)] = A'_j \text{sinc}(\pi t dv) \cos(2\pi v_j t + \phi_j), \quad (\text{A7})$$

where

$$A'_j = dv\epsilon_0 \sqrt{A_j} e^{-2\ln 2 \left(\frac{v_j - v_0}{\Delta v} \right)^2}. \quad (\text{A8})$$

The above formalism for a single frequency component from a discretized spectrum, can be extended to a frequency spectrum, $\epsilon(v)$, of n frequency components. The Fourier transform of a discretized frequency spectrum of n frequency components is the sum of the Fourier transform at each individual discretized frequency, j . Thus, the general form of the time domain laser pulse, $\epsilon(t)$, with the discretized form described by Eq. (2) is

$$\epsilon(t) = \text{sinc}(\pi t dv) \sum_{j=0}^n A'_j \cos(2\pi v_j t + \phi_j). \quad (\text{A9})$$

¹L. Vandersypen, M. Steffen, G. Breyta, C. Yannoni, M. Sherwood, and I. Chuang, *Nature (London)* **414**, 883 (2001).

²J. Jones and M. Mosca, *J. Chem. Phys.* **109**, 1648 (1998).

³I. Chuang, L. Vandersypen, X. Zhou, D. Leung, and S. Lloyd, *Nature (London)* **393**, 143 (1998).

⁴C. Sackett, D. Kielpinski, B. King, C. Langer, V. Meyer, C. Myatt, M. Rowe, Q. Turchette, W. Itano, D. Wineland *et al.*, *Nature (London)* **404**, 256 (2000).

⁵S. Gulde, M. Riebe, G. Lancaster, C. Becher, J. Eschner, H. Haffner, F. Schmidt-Kaler, I. Chuang, and R. Blatt, *Nature (London)* **421**, 48 (2003).

⁶H. C. Nägerl, D. Leibfried, H. Rohde, G. Thalhammer, J. Eschner, F. Schmidt-Kaler, and R. Blatt, *Phys. Rev. A* **60**, 145 (1999).

⁷D. Demille, *Phys. Rev. Lett.* **88**, 67901 (2002).

⁸L. Carr, D. Demille, R. Krems, and J. Ye, *New J. Phys.* **11**, 055049 (2009).

⁹C. M. Tesch and R. de Vivie-Riedle, *Phys. Rev. Lett.* **89**, 157901 (2002).

¹⁰T. Baumert, T. Brixner, V. Seyfried, M. Strehle, and G. Gerber, *Appl. Phys. B* **65**, 779 (1997).

¹¹R. Judson and H. Rabitz, *Phys. Rev. Lett.* **68**, 1500 (1992).

¹²B. Amstrup, G. J. Toth, G. Szabo, H. Rabitz, and A. Loerincz, *J. Phys. Chem.* **99**, 5206 (1995).

¹³J. Vala, Z. Amitay, B. Zhang, S. Leone, and R. Kosloff, *Phys. Rev. A* **66**, 62316 (2002).

¹⁴K. Hosaka, H. Shimada, H. Chiba, H. Katsuki, Y. Teranishi, Y. Ohtsuki, and K. Ohmori, *Phys. Rev. Lett.* **104**, 180501 (2010).

¹⁵K. Mishima and K. Yamashita, *Chem. Phys.* **367**, 63 (2010).

¹⁶J. L. Chen, C. M. Ling, C. C. Hwang, and Y. H. Ho, *J. Chem. Phys.* **134**, 134103 (2011).

¹⁷K. Shioya, K. Mishima, and K. Yamashita, *Mol. Phys.* **105**, 1283 (2007).

¹⁸M. Tsubouchi and T. Momose, *Phys. Rev. A* **77**, 052326 (2008).

¹⁹Z. Bihary, D. R. Glenn, D. A. Lidar, and V. A. Apkarian, *Chem. Phys. Lett.* **360**, 459 (2002).

²⁰Y. Ohtsuki, *Chem. Phys. Lett.* **404**, 126 (2005).

²¹W.-Z. Cao, L. J. Tian, H. J. Jiang, and C. Li, *Int. J. Quantum Inf.* **6**, 1223 (2008).

²²C. Menzel-Jones and M. Shapiro, *Phys. Rev. A* **75**, 052308 (2007).

²³K. Mishima, K. Tokumo, and K. Yamashita, *Chem. Phys.* **343**, 61 (2008).

²⁴K. Mishima and K. Yamashita, *Chem. Phys.* **361**, 106 (2009).

²⁵D. Sugny, L. Bomble, T. Ribeyre, O. Dulieu, and M. Desouter-Lecomte, *Phys. Rev. A* **80**, 042325 (2009).

²⁶M. Zhao and D. Babikov, *J. Chem. Phys.* **125**, 024105 (2006).

²⁷D. Babikov, *J. Chem. Phys.* **121**, 7577 (2004).

²⁸E. A. Shapiro, I. Khavkine, M. Spanner, and M. Y. Ivanov, *Phys. Rev. A* **67**, 013406 (2003).

²⁹Y. Teranishi, Y. Ohtsuki, K. Hosaka, H. Chiba, H. Katsuki, and K. Ohmori, *J. Chem. Phys.* **124**, 114110 (2006).

³⁰Y. Ohtsuki, *New J. Phys.* **12**, 045002 (2010).

³¹R. R. Zaari and A. Brown, *J. Chem. Phys.* **135**, 044317 (2011).

³²R. R. Zaari and A. Brown, *J. Chem. Phys.* **132**, 014307 (2010).

³³A. P. Peirce, M. A. Dahleh, and H. Rabitz, *Phys. Rev. A* **37**, 4950 (1988).

³⁴W. Zhu, J. Botina, and H. Rabitz, *J. Chem. Phys.* **108**, 1953 (1998).

³⁵C. Gollub, M. Kowalewski, and R. de Vivie-Riedle, *Phys. Rev. Lett.* **101**, 073002 (2008).

³⁶M. Schroeder and A. Brown, *New J. Phys.* **11**, 105031 (2009).

³⁷M. Lapert, R. Tehini, G. Turinici, and D. Sugny, *Phys. Rev. A* **79**, 063411 (2009).

³⁸A. Mantz, J.-P. Maillard, W. B. Roh, and K. N. Rao, *J. Mol. Spectrosc.* **57**, 155 (1975).

³⁹D. Goorvitch and C. Chackerian, *Astrophys. J., Suppl. Ser.* **91**, 483 (1994).

⁴⁰D. L. Carroll, Genetic Algorithm driver v1.7.0 (2004); see also at <http://www.cuaerospace.com/carroll/ga.html>.

⁴¹C. M. Tesch and R. de Vivie-Riedle, *J. Chem. Phys.* **121**, 12158 (2004).

⁴²N. Rosen and C. Zener, *Phys. Rev.* **40**, 502 (1932).

⁴³G. F. Thomas, *Phys. Rev. A* **27**, 2744 (1983).

⁴⁴M. Holthaus and B. Just, *Phys. Rev. A* **49**, 1950 (1994).

⁴⁵T. Cheng and A. Brown, *J. Chem. Phys.* **124**, 034111 (2006).